C/NOFS: a Mission to Forecast Scintillations

O. de La Beaujardière,
and the C/NOFS Science Definition Team:
Laila Jeong, Bamandas Basu, Santimay Basu,
Theodore Beach, Paul Bernhardt, William Burke, Keith Groves, Roderick Heelis,
Robert Holzworth, Cheryl Huang, Donald Hunton, Michael Kelley, Robert Pfaff,
John Retterer, Frederick Rich,
Michael Starks, Paul Straus, and Cesar Valladares

Submitted to Journal of Atmospheric, Solar-Terrestrial and Planetary Sciences
20 December 2002, Revised 16 July 2003

AIR FORCE RESEARCH LABORATORY
Space Vehicles Directorate
29 Randolph Road
Hanscom AFB, MA 01731

Abstract

This article describes the science to be pursued during the Communication / Navigation Outage Forecasting System (C/NOFS) Mission of the Air Force Research Laboratory. The primary purpose of C/NOFS is to forecast the presence of ionospheric irregularities that adversely impact communication and navigation systems. A satellite, scheduled for launch in January 2004 into a low inclination (13°), elliptical (~ 400 x 700 km) orbit, is the most significant component of the C/NOFS program. Complementary ground-based measurements are also critical to the success of the mission.

C/NOFS science objectives may be organized into three categories: (1) to understand physical processes active in the background ionosphere and thermosphere in which plasma instabilities grow; (2) to identify mechanisms that trigger or quench the plasma irregularities responsible for signal degradation; and (3) to determine how the plasma irregularities affect the propagation of electro-magnetic waves.

C/NOFS is the first satellite solely dedicated to forecasting ionospheric irregularities and radio wave scintillations. It will be equipped with sensors that measure the following parameters: ambient and fluctuating electron densities; ion and electron temperatures; AC and DC electric fields; magnetic fields; neutral winds; ionospheric scintillations; and electron content along the lines of sight between C/NOFS and the Global Positioning System (GPS). Thus, the sensor suite on C/NOFS is richer than on any previously flown equatorial satellite. A broad range of ground-based measurements will complement the space data. In addition, data from several other satellites and rocket experiments will augment the C/NOFS observations. Several campaigns are planned to validate operational forecasts, acquire data to achieve the science goals, and test the theoretical models.

We anticipate that by the end of the C/NOFS mission, our understanding of the physics controlling the equatorial ionosphere will have advanced to the point that we will be able to nowcast and forecast the formation of ionospheric irregularities to a high degree of accuracy. However, this is not an easy task because a 2 to 6 hour forecast is required, as well as an extended prediction – a three-day "outlook".

1. Introduction

Radio waves scatter as they propagate through plasma density irregularities in the ionosphere. Often, the resulting scintillation of signals reaching the ground significantly degrades the performance of transionospheric communication and navigation systems. Impacts can be particularly severe at low magnetic latitudes in the post sunset hours. The operational objective of the C/NOFS program is to develop reliable forecasts of the times and durations, locations, and magnitudes of outages that Air Force communication and navigation users will experience. We intend to address this operational need by assimilating satellite and ground-based measurements into physics-based space weather models. However, to meet the operational objective, we must first advance scientific understanding about the origins and nature of the low-latitude plasma turbulence that causes the outages. The science objectives of the C/NOFS mission are listed in Table 1 and fall into three broad categories:

1. Advance physical understanding of equatorial ionospheric plasmas at all local times, with a special emphasis on the post-sunset sector, as a basis for accurately forecasting the background ionosphere and the formation of scintillation-producing irregularities.

2. Identify critical processes that cause linearly unstable ionospheric plasmas to evolve into nonlinear plasma depletions and plumes associated with the most severe signal losses.

3. Model electromagnetic wave propagation through equatorial ionospheric plasma irregularities to estimate the intensities of phase and amplitude scintillations for signals at VHF through L band frequencies, at all local times and longitudes.

This paper first describes the C/NOFS mission and instrumentation. It then briefly describes the ambient ionospheric/thermospheric system in the low latitude region to introduce the main science issues. As listed in Table 1, these issues include: linear growth of plasma instabilities; sources of equatorial electric field; ambient ionosphere specification and forecast; nonlinear development of plasma irregularities; plasma turbulence spectrum; radio wave transmission through perturbed ionospheric plasmas to compute scintillation indices; and scintillation climatology. Section 6 is about coordinated ground and space observations. The final section includes a summary and conclusions. Additional details about the science questions to be addressed with C/NOFS, and about the collaborative ground and space observations are described in *de La Beaujardière et al*., 2003.

2. C/NOFS Instrumentation Payload and Mission Profile

Sensors on the C/NOFS satellite will provide information critical for driving global ionospheric forecast models. The satellite, illustrated in Figure 1, will fly in a 13° inclined orbit at altitudes between 400 and 700 km. This orbit keeps C/NOFS on magnetic field lines with apex altitudes ≤ 800 km about half the time, and between the ionospheric equatorial-anomaly crests most of the time. A unique aspect of the C/NOFS mission is that during its later phase, a subset of the environmental data and housekeeping telemetry streams will be transmitted through NASA's Tracking and Data Relay Satellite System (TDRSS) to drive predictive models in real time.

The satellite payload includes five *in situ* sensors and a multi-frequency beacon. Table 2 lists the satellite instruments, the principal investigators, and their institutions.

The Planar Langmuir Probe (PLP) is a dual-disk probe to monitor ionospheric plasma densities. PLP provides low time-resolution density inputs for background ionosphere models and high time-resolution density irregularity measurements to specify disturbance microphysics. Electron densities and temperatures will be used to help quantify environmental conditions that produce scintillations and model electron density profiles. PLP also monitors the spacecraft surface potential.

The Ion Velocity Meter (IVM) comprises two sensors, an ion drift meter and a retarding potential analyzer that will directly measure the ion drift vector, the ion temperature, and the major ion composition with a spatial resolution of about 4 km along the satellite track. The ion drift meter will also provide measurements of the local vertical and horizontal ion drift components with a spatial resolution of 500 m.

The Neutral Wind Meter (NWM) consists of two sensors, a cross track wind sensor (CTS) and a ram wind sensor (RWS) that will directly measure the neutral wind vector with a spatial resolution of about 8 km along the satellite track. Measurements will be made over a restricted altitude range between perigee and the exobase, which is dependent on solar activity levels during the mission.

The IVM and NWM instruments used as part of the C/NOFS program will also be used to conduct the Coupled Ion Neutral Dynamics Investigation (CINDI) sponsored by NASA. This collaborative endeavor between the Air Force and NASA is designed to maximize the science and operational capabilities of the instrumentation.

The Vector Electric Field Instrument (VEFI) primarily consists of three orthogonal 20 m tip-to-tip double probe antennas. VEFI will measure DC electric fields causing plasma drift motions that drive the ionosphere unstable. It will also measure quasi-DC electric fields within the plasma depletions to determine their motions relative to the background ionosphere. VEFI will measure vector AC electric

fields to characterize the microphysics of ionospheric irregularities. A fluxgate magnetometer, optical lightning detector, and fixed-bias Langmuir probe complete the VEFI instrument package.

The Coherent Electromagnetic Radio Tomography (CERTO) is a tri-band (150 MHz, 400 MHz, 1067 MHz) radio beacon. CERTO will be used in multi-frequency scintillation studies with ground receivers to specify plasma conditions between the location of C/NOFS and the Earth. It will also be used for tomographic reconstruction of electron density profiles.

The C/NOFS Occultation Receiver for Ionospheric Sensing and Specification (CORISS) is a Global Positioning System (GPS) dual-frequency receiver. CORISS will measure total electron content (TEC) along the lines-of-sight between C/NOFS and GPS satellites. It will thus provide a remote sensing capability for extracting vertical profile information during occultations (i.e., when GPS satellites are moving behind the Earth). Limb profiles of TEC can be inverted to produce vertical profiles of electron density. CORISS measurements of TEC from occulting and non-occulting GPS satellites at various bearings relative to the satellite track can constrain C/NOFS ionospheric models. It may also be possible to measure L-band scintillations caused by electron density irregularities along lines-of-sight between C/NOFS and GPS satellites. This technique is currently in an early stage of development.

A system of seven ground-based radio wave receivers called the Scintillation Network Decision Aid (SCINDA) has been installed to support the C/NOFS mission. As shown in Figure 2, SCINDA sites have been established at Ancon, Peru; Antofagasta, Chile; Ascension Island; Bahrain; Diego Garcia; Guam; Manila; and Singapore. SCINDA receivers monitor beacon signals from geostationary satellites to determine the amplitude scintillation index (S_4) using spaced antenna measurements to provide an estimate of the drift of ionospheric irregularities. The SCINDA sites also have GPS receivers to monitor amplitude and phase scintillations on all available GPS satellite links. Future upgrades include adding steerable antennas at selected SCINDA sites to track CERTO beacon signals from the C/NOFS satellite and to incorporate GPS TEC measurements.

The last component of the Mission is the C/NOFS Data Center. It will acquire the satellite data and telemetry, as well as the ground-based data and geomagnetic indices. It will process the data into physical parameters, and run the algorithms that nowcast and forecast the ionosphere and scintillation. The data center will display the results as maps of scintillation regions.

The mission profile calls for a first period in Survey Mode to refine the algorithms and test the products, and a second period in Forecast Mode, during which part of the satellite data will be acquired in real time in order to generate specification and forecast maps of the global ionosphere and scintillation levels. The real time data system is provided by NASA, and will make use of the TDRSS system. The equatorial ionospheric scientific investigations will take place during both Survey and Forecast Modes. The satellite-planned lifetime is five or more years.

3. Background Ionosphere and Thermosphere

In order to specify and forecast the onset of scintillations we must exploit the C/NOFS data to model the background ionosphere and thermosphere in which plasma irregularities grow. The morphology of the equatorial ionosphere is quite different from that at other latitudes because the magnetic field, **B**, is nearly parallel to the Earth's surface. During daytime, the E-region dynamo electric field (**E**) is eastward. An eastward electric field in the E region at off-equatorial latitudes maps along the Earth's magnetic field to F-region heights above the magnetic equator. As illustrated in Figure 3, the resulting **E** x **B** drift transports F-region plasma upward at the magnetic equator. The uplifted plasma then moves along **B** in response to gravity and pressure-gradient forces. As a result, the equatorial (Appleton) anomaly is formed with minimum F-region ionization density at the magnetic equator and maxima at the two crests approximately 15° to 20° in magnetic latitude to the north and south.

Near sunset, plasma densities and dynamo electric fields in the E region decrease, and the Appleton anomaly begins to fade. However, at this local time a dynamo develops in the F region. Polarization charges within conductivity gradients at the terminator enhance the eastward electric field for about an hour after sunset. The post-sunset electric field moves the ionospheric plasma upward, allowing the Appleton anomaly crests to intensify. Eventually the electric field turns westward, causing plasma to drift downward. Soon after sunset, vertical plasma density gradients form in the bottom side of the F layer. The upward density gradient is opposite in direction to the gravitational force. This configuration is Rayleigh-Taylor (R-T) unstable and allows plasma density irregularities to form. Eastward post-sunset electric fields enhance the R-T instability, while westward fields quench it. On some days the magnitude of **E** is insufficient to cause equatorial anomaly crests or ionospheric irregularities before its polarity reverses. These irregularities can grow to become large ionospheric depletions often called equatorial plasma bubbles. Note that the term "bubble" is misleading in that the depletions are not spherical but elongated along a magnetic flux tube.

An examination of the linear R-T growth rate provides insight as to how variability in background ionosphere-thermosphere conditions affects the formation of plasma irregularities. A description that takes into account the effects of plasma inhomogeneities along geomagnetic field lines, albeit in a simplified manner, is the flux-tube integrated description introduced by *Haerendel* [private, communication, 1973]. In this description, relevant plasma equations are integrated along equipotential field lines. A perturbation analysis is then applied to determine the linear growth rates. With some approximations, the linear growth rate γ for the flux-tube integrated, generalized R-T instability can be written as [*Sultan*, 1996]:

$$\gamma = \frac{\Sigma_P^F}{\Sigma_P^E + \Sigma_P^F}\left(V_p + U_n^P + \frac{g_L}{\nu_{in}^{eff}}\right)\frac{1}{L_n} - R_T \qquad (1)$$

Here g_L is the vertically downward acceleration due to gravity g at the magnetic equator and on a field line designated by the L (McIlwain parameter) value, so that

$$g_L = g_0 / L^2,$$

where g_0 is the value on the surface of the Earth. V_P, the vertically upward component of plasma drift due to the eastward electric field E_0 at the magnetic equator, is given by

$$V_p = cL^3 E_0 / B_0$$

where B_0 is the value of magnetic field B on the Earth's surface. U_n^P is the vertically downward component of neutral wind velocity perpendicular to B weighted by the flux-tube integrated Pedersen conductivity Σ_P. ν_{in}^{eff} is the flux-tube integrated effective F-region ion-neutral collision frequency, weighted by number density in the flux tube. L_n is the scale length of the vertical gradient of the F-region flux tube integrated plasma density, measured at the equator. R_T is the flux-tube integrated recombination rate. Σ_P^E and Σ_P^F are the contributions to the flux-tube integrated Pedersen conductivity from the E and F regions, respectively.

For the specified directions of **E**, U_n^P, and **g**, the growth rate γ of the generalized R-T instability can be positive only when L_n is positive. Under typical ionospheric conditions the growth period, 1/γ, is of the order of 10 minutes. It takes several growth periods for large-amplitude irregularities to grow.

Since g and B are constants at a given location, R-T growth rates are controlled by the variability of L_n, E_0, U_n^P, Σ_P^E, Σ_P^F, ν_{in}^{eff}, R_T and by the by the F-layer height, through the flux-tube integrated quantities. The fact that γ depends on the flux-tube integrated Pedersen conductivity, rather than its local value near the magnetic equator, proves to be critical for understanding the season versus longitude variability of bubble occurrence.

3.1 What are the Main Drivers of Equatorial Electric Fields?

Equation (1) indicates that **g**, **E,** and U_n^P control the R-T growth rate. The eastward electric field affects the growth rate in two ways: (a) it contributes directly to the growth rate, and (b) it elevates the F layer to altitudes where ν_{in}^{eff} is smaller, thus enhancing the growth rate-term associated with **g**. The height of the post sunset F layer at the magnetic equator is determined by the temporal history of the global electric field. Previous investigations have identified three possible sources of **E**: (1) dynamo action of neutral winds, (2) magnetospheric effects at low latitudes, and (3) gravity waves. Through analyses of C/NOFS data, we hope to model **E** with sufficient accuracy to identify its sources.

3.1.1 Dynamo Electric Field

The ordinary source of equatorial electrodynamics is the thermospheric dynamo that powers the equatorial electrojet [*Haerendel and Eccles*, 1992; *Eccles*, 1998]. An important aspect of the C/NOFS payload will be its ability to measure neutral and plasma winds directly, and thus help establish the accuracy and validity of existing thermospheric models. The time history of eastward electric fields before, during, and just after sunset determines the height of the dense post-sunset plasma. After sunset F-region dynamo currents are no longer subject to the shorting effect of the conducting E-layer to the north and south of the magnetic equator. Polarization fields are thus able to drive the F-layer upwards. Also, ν_{in}^{eff} in Equation (1) exponentially decreases with height. In the linear approximation, for every ~50 km of increased altitude the instability growth time decreases by a factor of e. Thus the height of the bottomside of the F-layer plays a key role in the appearance of severe scintillation, and knowledge of the behavior of the zonal electric field is crucial to a forecasting capability.

The plasma drift reverses from upward to downward near 1900 hrs. However, just before the drift reversal at the time of sunset, the drift is much enhanced [*Fejer et al*., 1999]. This is called the post-sunset or the pre-reversal enhancement (PRE) of the eastward electric field. The PRE causes rapid uplifting of the F region, and steepens the bottomside gradient leading to the R-T instability. (The vertical uplift of the plasma layer by the eastward electric field helps steepen the bottomside density gradient because the recombination frequency decreases exponentially with altitude as shown by Equation (24) in *Basu*, 1997).

PRE holds the key to the formation of irregularities and, therefore, the nowcasting and forecasting of irregularities and PRE are interrelated. The C/NOFS observations will help determine the main driver of the PRE and the parameters that control its magnitude.

The PRE at sunset is attributed to charge collection in the off-equatorial E region where the Hall conductivity reduces rapidly with local time. The eastward component of the neutral wind in the F region causes a downward E field (- **U x B**). This E field is smaller on the dayside because of larger E-region conductivity to which it is connected by the magnetic field. The electric field maps down to the E region and drives a westward Hall current in the E region. Owing to the much-reduced Hall conductivity on the nightside, the Hall current is much larger on the dayside. This results in a collection of negative charges at the terminator creating an eastward electric field enhancement on the dayside of the terminator [*Farley et al.,* 1986].

There are many contributions to the polarization charges that produce the PRE [*Eccles*, 1998]. In all cases the original driver is the meridional current perpendicular to the magnetic field driven by the F-region zonal wind. Large gradients in this current exist across the terminator and polarization charges accumulate at this interface. The resulting electric field peaks at this location modifying the plasma dynamics in ways that are not yet fully understood.

The conductivity of the ionosphere in magnetic contact with the unstable region is a critical quantity. In the laboratory, this is referred to as a conducting end plate that stabilizes flute-mode instabilities. However, this quantity is difficult to measure. It can be estimated from the ground using special ionosondes. In principle the CORISS instrument can measure E-region densities down to ~5×10^3 cm^{-3}, and may be able to approximate conductivity whenever GPS occultation geometries permit. In addition, *Kelley* [1989] has shown that if the Poynting flux is measured in bubble regions the end plate conductivity can be inferred. This should be possible using the electric and magnetic field sensors on C/NOFS.

With respect to the PRE, some of the questions to be addressed include:

- Can we establish the relative timing of west-to-east changes of the F-region neutral winds and the terminator-induced conductivity gradients? How strong is the eastward zonal neutral wind needed at the time of sunset?
- To the degree that F-region neutral winds are defined by tidal modes, is it possible to predict the behavior of the zonal component at sunset from daytime patterns?
- What is the relationship between the day-to-day variability of ionospheric irregularities and scintillations with the variability of neutral wind tidal modes?

The C/NOFS wind and EDP measurements just before and after sunset should allow reliable forecasts of scintillations. The EDP model derived from C/NOFS data will be useful for determining the height of the F layer and forecasting scintillation onset. The CINDI package will provide the most accurate neutral wind observations ever obtained from a satellite. Such observations have been very sparse. The C/NOFS satellite, in conjunction with ground-based observations, should provide breakthrough observations for specifying the role of neutral winds in equatorial aeronomy.

3.1.2 Penetration Electric Fields

Nishida [1968] found that ionospheric currents at polar cap and equatorial magnetic latitudes respond to directional changes of the interplanetary magnetic field (IMF) in identical ways. In the rest frame of the Earth, changes in the IMF appear as variations of the interplanetary electric field (IEF) that determines the rate of magnetic merging at the dayside magnetopause. The geoeffective portion of the IEF controls the potential imposed upon the polar cap [*Burke et al.*, 1999]. To support this potential drop Region 1, (R1) field-aligned currents (FAC) are drawn from the solar wind. R1 currents flow into the ionosphere on the dawn side of the polar cap and out on the dusk side. The continuity of ionospheric currents requires a distribution of electric potential throughout the global ionosphere [*Nopper and Carovillano*, 1978].

Ionospheric potentials map along magnetic field lines throughout the magnetosphere. Within the magnetosphere, electric fields transport and energize plasma sheet and ring current particles. If consequent plasma pressure gradients misalign with gradients in the magnetic flux-tube volume a second set of FACs, called Region 2 (R2), flows into (out of) the ionosphere in the equatorward part of the auroral oval in the evening (morning) magnetic local time (MLT) sector [*Vasyliunas*, 1970]. The potential distribution required for the continuity of ionospheric currents due to R2 has the opposite sense to that of the R1 FACs. The net effect is that R2 currents act to shield electric fields from the low-latitude ionosphere and from the conjugate magnetosphere earthward of the ring current's inner edge [*Senior and Blanc,* 1984*; Spiro et al.* 1988]. It takes several hours for the ring

current to develop after a sudden increase in the IEF and polar cap potential before shielding is complete. In the meantime the ring current acts as a high-pass filter allowing the IEF to influence the electric field structure at equatorial latitudes. Owing to the gradient in ionospheric conductivity near the dusk terminator, penetration electric fields in the evening sector have eastward components. . The low inclination ROCSAT-1 satellite data have been utilized to show that during major magnetic storms, the penetration of electric field into the equatorial ionosphere is confined to the longitude interval where rapid changes of Dst are occurring in the local dusk sector [*Basu et al.,* 2001a; *Basu et al.,* 2001b]. During penetration intervals, magnetospheric electric fields enhance and extend the domain of the destabilizing dynamo electric fields [*Fejer and Scherliess,* 1997 and references therein].

Recent studies using the Defense Meteorological Satellite Program (DMSP) satellites in the evening sector have demonstrated that intense, fast-moving equatorial plasma bubbles (EPBs) occur frequently in the initial and main phases of geomagnetic storms [*Huang et al.,* 2001]. Simultaneous measurements by the Combined Release and Radiation Effects Satellite (CRRES) in the inner magnetosphere indicate that penetration electric fields are responsible for triggering the creation of these structures [*Burke et al.*, 2000; *Wilson et al.*, 2001]. During the recovery phase of almost all storms, EPBs are not detected in the evening sector. They are, however, evident in the post-midnight to dawn MLT sectors. Bubble suppression in the evening sector and growth after midnight are attributed to the sustained action of a counter dynamo driven by Joule heating of the nighttime ionosphere/thermosphere at auroral latitudes [*Fejer and Scherliess,* 1997].

To take advantage of this knowledge for predicting EPB occurrence, it is necessary to recognize that penetration electric fields are controlled by the variability of the IEF. C/NOFS will help establish direct links between the IEF and electric fields in the low-latitude ionosphere. Solar wind and IMF data will be used to specify thresholds of the IEF needed to trigger EPBs. It will also be useful to compare Dst responses to IEF and solar wind pressure variations to establish criteria for predicting the end of the main and the beginning of the recovery phase of magnetic storms. This would provide all-clear signals for communication systems to resume normal operations. C/NOFS satellite data will be used to test numerical models of penetration electric field effects on equatorial electrodynamics.

3.1.3 Role of Gravity Waves, Tropical Storms, and Lightning

Gravity waves from the troposphere have long been considered an important source of energy transfer in the ionosphere/thermosphere system. A potential source of electric fields is plasma uplift in the post-sunset sector by gravity waves. The upward push due to these waves creates local zonal **U** x **B** currents alternatively east and west. These currents are not divergence-free and result in east and west electric fields. Recent studies of the PRE electric fields with the TIEGCM model [*Fesen et al.*, 2000] coupled to the mesospheric National Center for Environmental Prediction model suggest that the variability of the eastward electric field is modulated by the lower-altitude drivers. It has also been suggested that gravity waves propagating in the neutral atmosphere could act as seeds for EPBs [*Kelley et al.,* 1981; *Rottger,* 1981]. In this hypothesis, the postsunset ionosphere would be rising due to the thermospheric dynamo. Gravity waves could provide an extra push toward instability at a higher growth rate. *McClure et al.* [1998] argued that the global morphology of bubble occurrence suggests that tropospheric disturbances act as the main seeds for EPBs.

Recently, *Prakash* [1999] developed a theoretical model that only requires gravity-wave winds to couple to the E-region altitudes. Electric fields produced from gradients in the Hall conductivity couple to the F layer, and thus provide the seeds for bubble formation. This model predicts that gravity wave sources are at low latitudes. Therefore, meridionally propagating gravity waves from auroral disturbances cannot act as seeds for EPBs.

However, such gravity waves may be launched by tropical storm systems in the troposphere. The mechanisms responsible for upward energy propagation from tropical thunderstorms to initiate turbulence must be established in order to develop a successful predictive model. The C/NOFS database will provide the first means for establishing correlations between tropical storms and gravity

waves and/or their associated DC electric fields. The C/NOFS lightning detector on VEFI will provide signatures of storm activity to establish the statistical correlations. We will examine in particular the neutral motions and possible enhanced background DC electric fields that may be associated with tropospheric storms. Data from NASA's Tropical Rainfall Measuring Mission satellite have shown that flash rates increase exponentially with storm height [*Ushio et al.,* 2001].

Using Jicamarca incoherent scatter radar data, *Woodman and Kudeki* [1984] provided direct evidence for the explosive onset of plasma plumes resulting from lightning. NASA rocket flights directly over thunderstorms have now demonstrated the dramatic effects of lightning on ionospheric plasmas in the same altitude region as C/NOFS [e.g*., Kelley et al.,* 1985, 1989; *Li*, 1993; *Barnum,* 1999]. The mechanism for the energy deposition from lightning is under investigation, but the triggering itself is well documented. The C/NOFS mission is designed not only to monitor the occurrence of lightning-generated explosive plume development, but also to investigate the physical mechanisms responsible for the phenomenon. Lightning-related electric field waves originating as far away as 2500 km from the satellite sub-track can be detected by VEFI and captured optically by the lightning detector [*Holzworth et al.,* 1999].

The CORISS instrument provides another method of characterizing the presence of gravity waves generated by tropical storms. In addition to its primary function of providing ionospheric TEC measurements, CORISS is capable of measuring refractivity in the stratosphere/troposphere during the last ~30 seconds of a GPS occultation event. The refractivity observations may be converted into profiles of density and temperature. Gravity waves can be observed as fluctuations in these profiles. Thus, CORISS provides insight into the source region for locally generated gravity waves that may act as "seeds" for plasma instability. Recent examinations of GPS occultation data have established a connection between the occurrence of stratospheric temperature fluctuations and E-region irregularities.

3.2 Forecasting the Ambient Ionosphere

For our purposes, data assimilation will provide a snapshot of the ionosphere that will serve as initial condition for the ionospheric forecast model. The forecast model then will integrate forward in time to make predictions. For several decades now, sophisticated assimilation models have been used to forecast tropospheric weather. However, data assimilation techniques are only in their infancy when it comes to space weather specification and forecast. The C/NOFS satellite mission offers an opportunity to develop, test, and validate data assimilation techniques for the ionosphere and thermosphere.

3.2.1 C/NOFS Assimilation Models

Assimilation models provide the means to acquire snapshots of ionosphere/thermosphere structures using data from the C/NOFS satellite and other sources. The main problem to be addressed concerns data scarcity; a satellite provides only one-dimensional samplings of the parameters that are needed for a 3D specification of the Earth's ionosphere. Other issues that must be dealt with include recognizing data quality deterioration, nonsynchronicity of data delivery, data dropouts, and cold starts (without data).

Consider, for example, the assimilation of electric field data. To help achieve coverage of the ionospheric volume, geomagnetic field lines will be regarded as equipotentials at the relevant spatial scale. A vector measurement of the electric field at one point by the satellite thus provides the electric field at all points along the geomagnetic field line that intersects the observation point. As the satellite sweeps through its orbit, it measures the fields through the whole range of longitudes or local time. A model is required, however, to specify variations of the fields through the third dimension, field-line apex altitude. C/NOFS will determine how reliably predicted fields from previous forecasts can be used as prescriptions of the field variation with altitude.

As mentioned previously, gradients in the ion density in the bottomside of the ionospheric F layer are strong determinants of how vulnerable the plasma is to the R-T instability. Unfortunately, the satellite will rarely fly in this region, so we will be unable to measure bottomside gradients directly. The height of the bottomside gradient, however, strongly depends on the vertical velocity of the plasma, which is determined by electric fields. Latitudinal gradients in the plasma density are controlled by the interhemispheric neutral winds.

Data from the NWM will be assimilated to provide specifications of the winds. The main question then is to determine the degree to which the variability of dynamo winds can be used to explain how the variability of the vertical plasma drifts affects EPB occurrence.

The basic data-assimilation algorithm that will be employed in the C/NOFS data center involves the use of data to specify the drivers of an ionospheric forecast model. The model will integrate from a previous snapshot up to the present time to provide a current snapshot of the ionosphere. The code is based on the RIFS (Regional Ionospheric Forecast and Specification) model [*Eccles et al.*, 2000].

Electron density profiles derived from CORISS measurements may provide information about the height of bottomside density gradients and of E-region conductivities. The C/NOFS *in situ* ion sensors cannot estimate these quantities. CORISS slant path TEC observations of both the northern and southern anomaly crests may also provide sufficient information to constrain specification of neutral winds for modeling purposes. This would be particularly useful during times when the C/NOFS satellite is too high for the *in situ* neutral wind sensors to operate effectively.

The C/NOFS mission can provide one of the first real-time operational applications for the Global Assimilative Ionospheric Model (GAIM). A successful demonstration of GAIM, which is based on Kalman filter assimilation techniques, to specify the ambient ionosphere would be a revolutionary step toward ionospheric space weather prediction.

3.2.2 Ionospheric Forecasting

The ambient ionosphere forecast model begins with the snapshot of the ionosphere provided by the assimilation process and advances it through the forecast interval. The C/NOFS model will provide global coverage of both the plasma constituents and neutral thermospheric components of the ionosphere through the range of heights relevant for ionospheric processes, at a horizontal resolution of a few degrees in latitude and longitude. The C/NOFS data center will use the AFRL version [*Retterer et al.,* 2002] of the LOWLAT code [*Anderson,* 1973] to forecast ionospheric structure.

Forecasting the global ionospheric density is a major scientific challenge. The C/NOFS mission will help to (a) establish the degree to which models include the required physics, and (b) determine how far into the future simple extrapolations of the drivers provide accurate forecasts.

C/NOFS observations can also be used to validate other 3D ionospheric physics models, such as SAMI3 recently developed at NRL [*Huba and Joyce,* 2002]**.** This model treats the dynamic evolution of seven ion species (H+, He+, N+, O+, N2+, NO+, and O2+) in the altitude range 85 - 18,000 km. Thermal balance equations are solved for three ion species (H+, He+, and O+) and the electrons. The model includes ion inertia parallel to the geomagnetic field, as well as the radial and longitudinal E x B transport of the plasma. A time-splitting scheme is used: the dynamic of the system is first solved for motion along the geomagnetic field and then for motion transverse to it. The motion of the plasma along the geomagnetic field is described by advection/diffusion equations.

The C/NOFS measurements, especially the neutral winds, offer opportunities to validate theoretical self-consistent models of the coupled ionosphere/thermosphere such as the Thermosphere Ionosphere Electrodynamic General Circulation Model (TIEGCM) code developed by the team at NCAR, and the Coupled Thermosphere Ionosphere Model (CTIM) code developed by the team at the University of Colorado.

3.3 Equatorial Plasma Instabilities

An important element of the C/NOFS science plan is to identify the ionospheric conditions that lead to the onset of plasma instabilities, and to understand environmental processes that act to suppress onset. Forecasts of the background ionosphere will be examined to identify regions of R-T instability. An examination of these regions will form the basis for the forecast of the timing and the severity of radio scintillations.

The ionospheric plasma parameters that determine the onset and the growth of the plasma instability are highly variable both spatially and temporally. In spatially nonuniform plasmas, there are two key topological requirements for the onset of plasma instability. First, the plasma modes must have spatial profiles consistent with the physical regimes in which they are excited. Second, they must grow over the region of localization on realistic time scales without convecting away. In the equatorial ionosphere, the spatial variation of the electrical resistivity along the curved dipole magnetic field lines and that of density and ion-neutral collision frequency along the vertical direction help in realizing the localized modes [*Basu and Coppi,* 1983; *Basu and Coppi,* 1999]. On the other hand, the spatial variation of other plasma parameters can impose severe constraints that make the excitation of plasma modes topologically unfavorable, and so the instability may be inhibited [*Basu and Coppi,* 1999]. First-principle theoretical models will assist us in gaining quantitative understanding of the effects of the inhomogeneities of the various ionospheric parameters on the plasma instability mechanisms. This, in turn, will determine which plasma parameters have more influence than the others on the onset of the instability and so should play a more important role in the forecasting models.

Spatial profiles of the ionospheric plasma parameters are essential inputs for the study. Rocket measurements in coordination with the C/NOFS satellite measurements and other available ground-based (e.g., radar, ionospheric sounders) measurements will be useful in validating the concept and the models based on it.

Another important component of the C/NOFS plan is to develop a theoretical model that accurately calculates linear growth rates while incorporating pertinent plasma inhomogeneity effects. The linear growth model is needed to specify and forecast where in the equatorial ionosphere bubbles and plumes may occur with high probability. The description summarized in equation (1) takes into account the effects of plasma inhomogeneity, but it makes several simplifying assumptions. An accurate theoretical model must address the plasma inhomogeneity effects discussed above by adopting a more rigorous mathematical description. *Retterer et al.* [2002] have developed such a model, but it needs to be extended and validated through comparisons with C/NOFS observations.

A number of different assumptions can be made when performing linear instability analyses of ionospheric plasmas. Correlations of the theoretical predictions from various models will be made with the observed occurrence of bubbles. This allows meaningful discrimination between models and identification of assumptions that best characterize conditions under which perturbations grow.

C/NOFS measurements will also provide insights into the role of seeding or preconditioning of the plasma for irregularities to form. Much like the Atmospheric Explorer E observations of sizeable gravity waves in which plasma bubbles were found to form in the troughs [*Singh et al.,* 1997], C/NOFS observations of the ionosphere and thermosphere prior to the formation of bubbles will provide insight into the processes and conditions preceding bubble onset.

4. Nonlinear Bubble Development

Radar detections of plasma irregularities [*Woodman and La Hoz*, 1976] and satellite encounters with density depletions [*Burke et al.*, 1979] at altitudes well above the peak of the F layer indicated that linear descriptions of the R-T instability at equatorial latitudes were incomplete. Equation (1) restricts

positive growth rates to places where L_n is positive. Above the peak of the F layer L_n reverses sign. However, instead of slowing and decaying, very deeply depleted bubbles move upward at supersonic speeds and are regularly seen in the evening sector [*Hanson et al.*, 1997], especially during periods of high geomagnetic activity [*Huang et al.*, 2001]. *Ott* [1978] and *Anderson and Haerendel* [1979] followed the development of the R-T instability into the nonlinear regime and showed that indeed plasma bubbles are able to break into the topside ionosphere. Depending on the direction of the background **E** they may move upward, downward, or stagnate.

The R-T instability is responsible for the onset of upwelling depleted flux tubes that carry with them a broad spectrum of associated plasma irregularities that evolve as the flux tube rises and bifurcates. These irregularities result from a hierarchy of processes that depend both on their location within the bubble (e.g., along its walls or in the middle of the depletion) and their altitude, since the background neutral density affects the collision and diffusion terms in the dispersion relation. A whole range of key science issues concern the processes that act in the nonlinear development of the density depletions, and the plasma turbulence within them.

While force balance requires that large-scale irregularities align with the geomagnetic field, this does not preclude bifurcations and irregular shapes perpendicular to the field. As an example, Figure 4 shows a fully developed structure in an image taken from the Air Force facility at the top of the Haleakala volcano. The emission is from the (777.4 nm) oxygen recombination line. The airglow depletions are most turbulent and map along field lines to locations north of Hawaii. Severe scintillations accompany such signatures as seen in the lower plot, which shows the S_4 index from the GPS data taken in Hawaii.

Because of the tilt between the geomagnetic field and the C/NOFS satellite's low earth orbit, the satellite will sample ionospheric bubbles at a variety of positions along their latitudinal extent, as well as at various altitudes and local times. Thus, these data, as they accumulate over time, will give us a statistical picture of the structure of EPBs. We will be able to resolve the following questions:

- How buoyant are the bubbles in the ionosphere (and thus how high will they rise)?
- How far along the geomagnetic field lines do they extend?
- How are they structured by bifurcation caused by plasma instabilities?
- How are they sheared by structure in the forces that drive them (e.g., neutral winds), etc.? Shorter-scale electric fields from the vicinity of the bubbles will be used to describe how these structures move.

Other questions to be addressed include:

- Can the bubble velocity be used to predict how the bubbles drift and thus provide a short-term forecast of the location of scintillations?
- Will vertical plasma drifts within bubbles indicate how high they will rise, and thus to what latitudes the effect of their turbulence will be seen?

The irregularities within the bubbles are generally characterized as a broad spectrum of two-dimensional plasma turbulence. The spectral distribution of irregularities includes a broad component associated with waves that have undergone a non-linear cascade process, as well as spectral features associated with drift waves. Current thinking is that structures cascade from large to small scale by wave-wave coupling mechanisms, but drift waves and other distinct instability processes contribute to this distribution of collective unstable scale lengths [*Kelley et al.* 2002]. Accurate vector electric field and plasma density measurements, such as those available from the C/NOFS satellite, will enable the different wave contributions and cross-scale coupling processes to be ascertained for the first time under a wide variety of driving conditions. Ultimately, questions concerning the energy transfer between scale lengths, inverse cascades, and the wave anisotropy/isotropy distributions, which are

presently not understood, will come into focus with the advent of the new, comprehensive C/NOFS data set. These new observations will enable the irregularities at all scales to be understood in fundamental new ways.

The plasma irregularities are electrostatic; they contain ΔN and $\Delta\mathbf{E}$ components (similar to electromagnetic waves that contain $\Delta\mathbf{B}$ and $\Delta\mathbf{E}$ components). The density component of the irregularities may be directly related to the scattering mechanism that causes scintillations, as it represents the change in the refractive index of the medium through which the waves are propagating. However, since ΔN is a scalar, it contains no information concerning the direction of the plasma waves. The electric field wave measurements, on the other hand, provide the direction of the plasma waves since, for the electrostatic case, the direction of the wave vector, **k,** is parallel to $\Delta\mathbf{E}$. The magnitude of **k** is given by $2\pi/\lambda$, where λ is the wavelength. Characterizing the direction of the wave vector, **k**, is essential both for understanding the instability mechanisms that cause the irregularities and also for converting the observed plasma wave frequencies in the satellite frame to wavelengths.

As the direction of the plasma waves is critical to assigning a wavelength to the measured frequency, it will be particularly important for revealing the intensity of the plasma waves in directions that are not along the spacecraft velocity, for example, along the depletion walls, which can extend scattering effects beyond those expected for a thin screen. Such vertical and oblique scattering screens may be very effective in causing scintillations for signals propagating at different angles to the observer.

The C/NOFS VEFI also includes interferometer channels that permit the direct measurement of the phase velocity of the plasma waves as well as direct and more precise measures of their wavelengths.

In order to understand the different plasma waves associated with irregularities, it is necessary to measure *both* the electric field and plasma density simultaneously to understand their growth and energy sources. This must be carried out as a function of wavelength and angle with respect to the magnetic field.

The electric field spectra are often much shallower at the shorter wavelengths than the density spectra [*Hysell et al.,* 1994]. In these cases, since the density component falls off more steeply, the amount of signal present in the electric field component is much larger and, therefore, easier to detect at the shorter scales. Thus, the electric field probes are more sensitive at short wavelengths (< 50 m), and will be used to characterize the contributions at shorter scales. For this reason, the C/NOFS VEFI will routinely include spectral information at frequencies up to 16 kHz (~0.5 m), with extensions to even shorter scales possible. The shorter scale irregularities may directly scatter and affect radio wave propagation due to Bragg scatter for cases where the cm-scale wavelength is one half that of the direct carrier signal (~GHz frequencies). The complete spectra for electric field and density data will be sampled via the VEFI burst memory and will provide snapshots of the complete wave and spectral characteristics in regions of intense turbulence.

By extending the wave measurements to include the shorter scale waves, the measured spectral distributions provide the complete irregularity spectrum. As noted below, they provide evidence for direct scattering processes that are different from those associated with simple Fresnel scattering.

When analyzed as functions of driving conditions (e.g., DC electric field, plasma density depletion amplitude, altitude, etc.), these spectra are expected to reveal new features of the irregularities themselves and their source mechanisms, improving our ability to predict their presence in a variety of nighttime ionospheres.

To carry out these predictions, the ambient ionospheric/thermospheric conditions forecast by the global ionospheric models will serve as a background for a mesoscale model of the formation and evolution of plasma bubbles in the low-latitude ionosphere. Based on the principles of the pioneering NRL model [*Zalesak et al.*, 1982], this new nonlinear model [*Retterer*, 1999] describes the development of structures on scales from a few km to hundreds of km, including the onset of the R-T instability and its saturation as bubbles develop and rise through the F layer. The simulations give us

power spectra of the density irregularities, which we can extrapolate into the regime where they affect radio wave propagation to estimate the strength of scintillations they produce.

The C/NOFS mission will help develop our understanding of how irregularities are triggered and how they evolve. The plasma wave spectra are vital in this area, as they demonstrate how "active" a given density depletion is in generating plasma waves that might subsequently scatter radio waves. For this reason, we now include temporal evolution in our characterization of the plasma depletions and associated irregularities. The waves will be characterized as "fresh", "middle-aged", and "old" irregularities. All have very different characteristics, particularly with respect to the extent that they cause communication and navigation outages. Thus, characterizing irregularities associated with different evolved states of the depletions requires new approaches to advance the predictive capability of the models to a new level.

Finally, there are several scientifically important features of equatorial irregularities that we presently do not understand, but that may become clear with the aid of the data gathered in the C/NOFS investigations. For example, we do not understand at what unstable scale sizes energy is injected and at what scales it is dissipated. Further, how does this energy couple between scale sizes, and at what wavelength regime is this accomplished most efficiently? We do not understand peaks in plasma wave spectra that consistently occur near 1 km or the presence of sub-meter scale waves and whether they are important for scattering GHz transmissions. By using the wave spectra to examine the whole picture of the ionospheric irregularities, we can expect to understand the underlying principles of how the irregularities form and, ultimately, how they scatter and disrupt radio wave propagation.

5. Plasma Irregularities and Radio Wave Scattering

In order to establish both causal and predictive relationships between ionospheric irregularities and communications / navigation outages, a series of steps must be advanced. Assume that we can characterize irregularity spectra as functions of ionospheric driving conditions and have predicted the strength and plasma wave characteristics of irregularities. The final steps are to understand how the irregularities enable different scattering processes to alter radio wave transmissions and produce phase/amplitude signal degradation and to evaluate the relative efficiencies of these processes at different frequencies or wavelengths, in order to predict the degree to which they disrupt communication links.

5.1 Fresnel and Bragg Scattering

There are a number of processes that scatter and/or alter radio waves, consequently disrupting communication and navigation systems within a wide range of carrier frequencies (wavelengths). For example, the dominant phase scintillation process at work in the unstable equatorial ionosphere is Fresnel scattering. In the Fresnel scattering approximation, plasma density irregularities with horizontal scale lengths of ~100 m in a thin screen at ~400 km altitude contribute the bulk of the weak scatter effects at GHz radio wave frequencies. The shape of the power law spectrum of the irregularities is a critical factor in determining the efficiency and scale lengths of ionospheric scatter via the Fresnel process. Furthermore, although Fresnel scattering for overhead sources is generally caused by a thin layer of horizontally oriented plasma waves, vertically propagating disturbances along the walls of the unstable flux tubes may also give rise to Fresnel scattering, affecting, in particular, radiowave sources that are not directly overhead.

Beyond Fresnel scattering, direct Bragg scattering operates when the wavelength of the density irregularity is half that of the radio wavelength. For HF communications, such scatter occurs at tens of meters, which corresponds to scale lengths found in typical spread-F irregularity spectra. In the case of strongly driven situations, irregularities may be driven to sub-meter scales, implying that it is also possible that Bragg scattering may directly affect radiowaves with wavelengths of tens of cm,

corresponding to frequencies up to a few GHz. Indeed, the frequency spectrum over which Bragg scattering might influence radio propagation is currently not known, nor is the severity with which such effects might occur. Data from the C/NOFS satellite will be used to advance our understanding of the degree to which these different scattering mechanisms operate as a function of wavelength.

5.2 Phase Screen Theory

The C/NOFS team has selected a phase screen approach for estimating scintillation statistics in both the specification and forecast modes. The limited amount of data available from the spacecraft drives this choice. As the spacecraft passes through an irregularity structure, it provides one-dimensional measurements of the medium.

The phase screen approach is particularly suited to one-dimensional data sets because, at least at the mathematical level, it requires only a one-dimensional parameter if the structures are greatly extended along magnetic field lines. The screen at any one point is characterized by the TEC along the line-of-sight between orbital and terrestrial transceivers. Variation in TEC along the line-of-sight causes a phase shift to be imparted to an initially uniform plane wave impacting the infinitesimally thin screen at some altitude. The resulting phase perturbations lead to diffraction and amplitude scintillations as the wave passes beyond the screen to the receiver. The scintillations are computed under a forward-scatter approximation [*Rino,* 1979]. This technique is broadly applicable under many ionospheric scintillation conditions, but cannot be used to model multiple-scatter and wide-scatter screen effects.

Figure 5 illustrates the steps that are planned to calculate the scintillation parameters. The reduction of sampled densities to power spectra allows us to create different realizations of the irregularity structure while preserving the overall frequency content and distribution. To create a density realization at a given location, we recreate the phase information of the Fourier Transform. This is typically accomplished with a random phase function, the most noticeable effect of which is the absence of sharp gradients in the resulting density waveform. It is not known how significantly this loss of structure affects scintillation estimates, apart from a few specific cases.

Once the necessary density realizations have been generated, appropriate modifications for the expected correlation lengths (and heights) of the irregularity plume and large-scale irregularity amplitude assumptions can be applied. The best models for these characteristics are not known. The set of density waveforms is finally collapsed into the parameter NT (x), converted to phase angle, and a solution is propagated through the phase screen. Scintillation statistics are gathered from the waveform produced after propagation through and away from the screen.

5.3 Phase Screen Science Issues

Open questions that bear on the phase screen approximation include the following: What is the correlation of observed scintillations from LEO beacons with scintillations observed from GEO satellites transmitting through a common volume? This correlation is not well known. Scintillations affecting beacons in LEO apply to spherical wave fronts, while those affecting GEO satellites impact largely planar wave fronts. The direct mapping of effects from one case to the other is not understood. Data from CERTO beacons and GEO spacecraft transmitting through a common volume can be compared to answer this question.

The effects of amplitude and phase scintillations at different frequencies are known to vary. The thresholds at which each type of scintillations become problematic for different applications are largely unknown. A critical aspect of the long-term usefulness of C/NOFS lies in understanding the required granularity of the specification and forecast products. This effort requires field-testing of a variety of different pieces of equipment in different scintillation environments.

Current research efforts are examining improved techniques for estimating scintillations from limited data sets. Examples of this include discrete versions of the Huygens-Fresnel integrals [*Costa and*

Basu, 2002], improved parabolic equation solvers, and sub-sampled phase screen work [*Beach et al.* 2002]. Insights gained from each of these efforts may lead to dramatic improvements in estimation accuracy and efficiency. These techniques can be evaluated in the same manner as the current phase screen approach. Scintillation estimates based on *in situ* data should be compared to statistics measured by ground facilities to assess each algorithm's performance.

6. Improved Scintillation Climatology

The morphology of equatorial scintillations, based primarily on 250 MHz observations and some 1.5 GHz geostationary satellite measurements, is well summarized in several publications [*Aarons,* 1982; *Basu and Basu,* 1985; *Aarons,* 1993]. These and other observations have been combined to form an empirical model called Wide-Band Model (WBMOD) [*Secan et al.* 1995]. The C/NOFS mission will offer the opportunity to improve and expand this model. The extensive GHz GPS scintillation measurements with the SCINDA sites [*Groves et al.,* 1997] have provided a deeper insight into the earlier scintillation morphology.

The morphology of equatorial density irregularities has been studied by several authors – for example, *Kil and Heelis* 1998 using the Atmosphere Explorer-E satellite, and *Huang et al.* 2002, using the DMSP satellite. These studies have shown that the root causes for the longitudinal and seasonal variations are still poorly understood. The C/NOFS satellite will provide data that can quantify the role of parameters such as winds, seeding from below, magnetic field intensity, and conductivities to explain the longitudinal, seasonal and solar cycle variability.

The latitudinal extent of equatorial scintillations typically ranges between ~15^o north and 15^o south magnetic latitudes. This corresponds to the region between the northern and the southern crests of the equatorial anomaly in F-region ionization. The belt width varies with solar cycle and is generally narrower during solar minimum and wider in solar maximum. The width also exhibits day-to-day variability. By mapping the extremes of the scintillation belt along magnetic field lines to the magnetic equator, the altitude extent of the irregularities at the magnetic equator can be determined. A scintillation belt width of 15^o magnetic latitude corresponds to an altitude extent of irregularities to ~750 km above the magnetic equator. Due to a finite upwelling speed of irregularities at the magnetic equator, scintillations near the crest of the anomaly may be delayed by 60 to 90 minutes from their onset at the equator.

The magnitude of amplitude scintillations is expressed by a scintillation index, S4, that is defined by the ratio of the standard deviation of signal intensity fluctuations and the average signal intensity. The index varies from zero to its saturated value that ranges between 1.0 and 1.5. The magnitude of amplitude scintillations decreases with increasing frequency. When scintillations are weak (S4 < 0.6), this variation is expressed by $S_4 \propto f^{-1.5}$, where f is the frequency. When scintillations are strong, the exponent of the frequency dependence decreases. For operational systems, the depth of fading of the signal intensity in decibels is more useful. For reference it may be noted that 6 dB fading corresponds to S4 ≈ 0.4, and 12 dB fading corresponds to S4 ≈ 0.7.

The C/NOFS mission will provide information on how scintillations vary as a function of an extensive set of parameters such as season, solar cycle, magnetic activity, density, electric fields, wind, etc. This climatology will yield valuable relationships and will also quantify the deviations from these average relationships as well as the expected variability of each parameter. The C/NOFS observations will also provide information about the persistence of scintillation, and its day-to-day variability. These studies will be essential to provide a long-term scintillation outlook more accurate than simple climatology.

The seasonal variation of equatorial scintillations is found to be a function of longitude. At lower frequencies, such as 250 MHz, scintillation activity maximizes in the equinoxes and one of the

solstices. Between 80° W and 80° E longitude, spanning South America and India, scintillation activity is maximum from September through April including the December solstice. In the Pacific sector, between 100° E and 170° W, spanning the longitudes of the Philippines and Kwajalein Island, the scintillation season covers the equinoxes and the June solstice. Thus, the solsticial patterns in these two sectors are opposite to one another. *Maruyama and Matuura* [1984] suggested that this effect is due to the trans-equatorial wind, which creates an asymmetric electron density variation around the magnetic equator and suppresses the growth of the R-T instability. In order to explain the phenomenon, *Tsunoda* [1985] advanced an alternate hypothesis that irregularities are likely to develop when the longitudinal gradient of magnetic field line integrated Pedersen conductivity is maximum at the time of sunset. In view of the variation of magnetic declination with longitude, the terminator aligns with the magnetic meridian at different longitudes in different seasons. This explained the seasonal pattern of scintillations at many longitudes. The problem with the hypothesis is that it does not predict the solsticial asymmetry of scintillations.

At higher frequencies, such as at L-band frequencies, scintillations at all longitudes occur primarily during the equinoxes and the solsticial activity is either absent or is similar to that of 250 MHz, but at a low marginal level. The frequency dependence of the seasonal variation of scintillations is an outstanding issue. C/NOFS will determine if the equatorial irregularities during the solstices are weaker than during the equinoxes.

In addition to plasma bubbles that are caused by the R-T instability, there is a distinct class of equatorial irregularities known as bottomside sinusoidal (BSS) irregularities [*Valladares et al.,* 1983]. The *in situ* density structures of BSS irregularities show a quasi-sinusoidal pattern, and the vertical drifts associated with the irregularities are mostly anti-correlated with the density structures. The one-dimensional spectrum of BSS irregularities is of the gaussian form with a scale size of ~1 km, not at all similar to the multi-component power law that is associated with EPBs. The BSS irregularities can cause strong VHF scintillations [*Basu et al.,* 1986] but only marginally affect GHz frequencies. These irregularities maximize during solstices, so that in the 250 MHz range, scintillation morphology at an equatorial station is determined by considering occurrence characteristics of both bubble type and BSS irregularities. The C/NOFS observations will provide a climatological model for BSS and clarify mechanisms of BSS formation.

The prime unknown of scintillation morphology is its extreme day-to-day variability. The major scintillation activity in the equatorial region is observed under magnetically quiet conditions. The day-to-day variability of scintillations needs to be examined in the context of neutral wind variations and its dependence on high latitude electrodynamics. C/NOFS will provide the rare opportunity to understand the statistical relationships between irregularities, winds, and global circuits.

7. Coordinated Ground-Based and Satellite Measurements

Ground-based instruments play three different roles in the C/NOFS program: (1) to provide real time data for scintillation and ionospheric models and predictions, (2) to validate the AF operational algorithms, and calibrate the instruments, and (3) to support scientific investigations requiring satellite and ground-based observations.

Instruments most relevant to the C/NOFS mission include incoherent scatter radars, coherent scatter radars, digital ionosondes, magnetometers, Fabry-Perot interferometers, and optical imagers. In addition, GPS, UHF-scintillation, and satellite-beacon receivers constitute the backbone of the CNOFS ground instrumentation.

A vigorous program of ground-based observations is planned for C/NOFS, including several observation campaigns. Of special interest, will be a rocket campaign in Kwajalein. The success of C/NOFS and follow-on operational systems ultimately depends on how completely we understand the

equatorial ionosphere. Many of the research questions outlined in the C/NOFS Science Plan can best be answered by combining the satellite data with observations from ground instruments.

New instruments will be designed and deployed in conjunction with C/NOFS to complement the science program. These instruments include special ionosondes to measure low plasma densities at night, Fabry Perot Interferometers, airglow all-sky cameras that can acquire data during the day and at night, as well as arrays of receivers for tomographic reconstruction.

Satellites will also provide complementary observations. Several that are expected to play a major role in the C/NOFS program include DMSP, ROCSAT, TIMED, COSMIC, GRACE, and EQUARS, among others. Remote sensing instruments such as the UV imagers on DMSP and TIMED and the GPS occultation sensors on COSMIC will be of particular interest because of their wide coverage. Data from these satellites will be used to validate the C/NOFS-derived parameters and forecast algorithms by providing additional data that can be assimilated into the models. By extending the coverage in latitude, longitude, and height, satellites will also make available a more complete ionosphere and thermosphere characterization.

8. Summary and Conclusions

The C/NOFS satellite is scheduled to be launched in January 2004 into a low inclination (13^o), low altitude elliptical orbit (~400 x 700 km). The satellite instruments include:

- Planar Langmuir Probe (PLP)
- Vector Electric Field Instrument (VEFI)
- Ion Velocity Meter (IVM)
- Neutral Wind Meter (NWM)
- GPS dual-frequency receiver (CORISS)
- Coherent radio beacon (CERTO)

C/NOFS ground-based instruments include scintillation receivers as well as GPS receivers to measure TEC and L-Band scintillation. In addition, data from other ground-based instruments such as optical instruments, ionosondes, Fabry Perot Interferometers, and radars will complement the mission.

The mission first period is in Survey Mode to test, and validate the algorithms, and the second period is in Forecast Mode, during which part of the satellite data will be acquired in real time in order to generate operational real-time products. The scientific investigations will take place during both Survey and Forecast Modes.

The science objectives are summarized in Table 1, along with, for each category the most pressing questions. In short, the science will be aimed at the following:

1. Understand the physics of the ionospheric plasma in the equatorial regions. The goal is to specify and forecast the background ionosphere accurately. This implies that the ionospheric drivers – ionospheric as well as thermospheric parameters – need to be specified and forecast. It also implies generating improved scintillation climatology.
2. Understand the physical processes that lead to the formation of plasma irregularities in the ionosphere, and identify the mechanisms that trigger or inhibit plasma instability. This goal implies accurate modeling of the parameters that are part of the instability growth rate. The electric field, whether of dynamo or magnetospheric origin, is one of the most important of these parameters. This goal also entails physics-based modeling of plasma bubbles and their time evolution.

3. Characterize spread-F irregularities and model the propagation of radio waves through the ionosphere in order to estimate the phase and amplitude scintillations for various propagation geometries. This goal implies the understanding of the irregularity spectra, of the cascading processes, as well as the construction of appropriate phase screens.

One of the innovative features of C/NOFS is that most of the scientific effort will be directed towards forecasting. An attempt will be made to foresee ionospheric and plasma irregularity parameters as far as 6 or even 72 hours ahead.

The science objectives cannot be met by using the satellite data alone. Theory and modeling are also required, as well as ground-based and other satellite observations. Synchronized efforts using many instruments, coordinated campaigns, theory, and data analysis are essential.

The maximum benefit can only be met if resources from other agencies such as NSF, NASA, the Office of Naval research, and AFOSR are applied. In addition, the effort is based on extensive international collaborations. The benefits gained from such synergies have been demonstrated on many occasions. Recent examples include the Guest Investigator program for the NASA Dynamics Explorer mission, and the TIMED ground-based component initiative. Multi-instrument studies with C/NOFS will provide results that would be unattainable otherwise. The C/NOFS mission will provide to the science community the most extensive set of satellite instruments dedicated to equatorial aeronomy and scintillation studies. This opportunity should not be missed.

The prospects for scientific achievement with C/NOFS are substantial. We anticipate that at the end of the C/NOFS mission, our understanding of the physics of the equatorial ionosphere will have advanced to the point that we can nowcast and forecast the formation of ionospheric irregularities with greatly improved accuracy.

Acronyms

AFOSR	Air Force Office of Scientific Research
BSS	Bottomside Sinusoidal
CERTO	Coherent Electromagnetic Radio Tomography
CINDI	Coupled Ion Neutral Dynamics Investigation
CORISS	C/NOFS Occultation Receiver for Ionospheric Sensing and Specification
CTS	Cross Track Wind Sensor
DMSP	Defense Meteorological Satellite Program
GPS	Global Positioning System
IEF	Interplanetary Electric Field
IVM	Ion Velocity Meter
NASA	National Aeronautics and Space Administration
NWM	Neutral Wind Meter
PLP	Planar Langmuir Probe
ROCSAT	Republic of China Satellite
RPA	Retarding Potential Analyzer
R-T	Rayleigh-Taylor
RWS	Ram Wind Sensor
SCINDA	Scintillation Network Decision Aid
TEC	Total Electron Content
VEFI	Vector Electric Field Instrument

References

Aarons, J., Global morphology of ionospheric scintillations, *Proc. IEEE, 70,* 360, 1982.

Aarons, J., The longitudinal morphology of equatorial F-layer irregularities relevant to their occurrence, *Space Sci. Rev., 63,* 209, 1993.

Anderson, D. N., A Theoretical study of the ionospheric F region equatorial anomaly, I. Theory, *Planet. Space Sci., 21*, 409, 1973.

Anderson, D. N., and G. Haerendel, The motion of depleted plasma regions in the equatorial ionosphere, *J. Geophys. Res.*, *84*, 4251, 1979.

Barnum, B. H., Electromagnetic and optical characteristics of lightning measured in the earth's ionosphere, Ph.D. thesis, University of Washington, 1999.

Basu, B., and B. Coppi, Localized plasma depletion in the ionosphere and the equatorial spread F, *Geophys. Res. Lett., 10*, 900, 1983.

Basu, B, Generalized Rayleigh-Taylor instability in the presence of time-dependent equilibrium, *J. Geophys. Res., 102,* 17305, 1997

Basu, B., and B. Coppi, Relevance of plasma and neutral wind velocities to the topology and the excitation of modes for the onset of the equatorial spread F, *J. Geophys. Res., 104*, 225, 1999.

Basu, S., and K. M. Groves, Space Weather, *Geophys. Monograph 125,* 423, 2001.

Basu, S., Su. Basu, C. E. Valladares, A. Dasgupta, and H. E. Whitney, Scintillations associated with bottomside sinusoidal irregularities in the equatorial F region, *J. Geophys. Res., 91,* 270, 1986.

Basu, S., Su. Basu, K.M. Groves, H.-C. Yeh, S.-Y. Su, F.J. Rich, P.J. Sultan, and M.J. Keskinen, Response of the equatorial ionosphere in the South Atlantic region to the great magnetic storm of July 15, 2000, Geophys. Res. Lett., 28, 3577, 2001a.

Basu, Su., S. Basu, C.E. Valladares, H.-C. Yeh, S.-Y. Su, E. MacKenzie, P.J. Sultan, J. Aarons, F.J. Rich, P. Doherty, K.M. Groves, and T.W. Bullett, Ionospheric effects of major magnetic storms during the International Space Weather Period of September and October 1999: GPS observations, VHF/UHF scintillations, and in situ density structures at middle and equatorial latitudes, J. Geophys. Res., 106, 30,389, 2001b.

Basu, Su., and Basu, S., Equatorial scintillations, Advances since ISEA-6, *J. Atmos. Terr. Phy., 47,* 753, 1985.

Beach, T. L., T. R. Pedersen, M. J. Starks, and S.-Y. Su, Estimating the amplitude scintillation index from sparsely sampled phase screen data, submitted to *Radio Sci*., 2002.

Burke, W. J., D. E. Donatelli, R. C. Sagalyn, and M. C. Kelley, Observations of low-density regions at high altitudes in the topside equatorial ionosphere and their interpretation in terms of equatorial spread-F, *Planet. Sp. Sci.*, *27*, 593, 1979.

Burke, W. J., D. R. Weimer, and N. C. Maynard, Geoeffective interplanetary scale sizes derived from regression analysis of polar cap potentials, *J. Geophys. Res.*, *104*, 9989, 1999.

Burke, W. J., A. G. Rubin, N. C. Maynard, L. C. Gentile, P. J. Sultan, F. J. Rich, O. de La Beaujardière, C. Y. Huang, and G. R. Wilson, Ionospheric disturbances observed by DMSP at middle to low latitudes during the magnetic storm of June 4 - 6, 1991, *J. Geophys. Res.*, *105*, 18,391, 2000.

Costa, E. and Sa. Basu, A radio wave scattering algorithm and irregularity model for scintillation predictions, *Radio Sci.,* 37, doi: 10.1029/2001RS002498, 2002.

De La Beaujardière, O. et al., Communication / Navigation Outage Forecast System (C/NOFS) Science Plan, AFRL-VS- TR-2003-1501, 2003.

Eccles, J. V., Modeling investigation of the evening prereversal enhancement of the zonal electric field in the equatorial ionosphere, *J. Geophys. Res.*, *103*, 26,709, 1998.

Eccles, J. V., R. W. Schunk, and J. J. Sojka, Regional Ionospheric Forecast and Specification (RIFS) for Low-Latitude Navigation and Communications, AFRL technical report AFRL-VS-TR-2000-1579, 2000.

Farley, D. T., E. Bonnelli, B. G. Fejer, and M. F. Larsen, The prereversal enhancement of the zonal electric field in the equatorial ionosphere, *J. Geophys. Res.*, *91*, 13,723, 1986.

Fejer, B. G., and L. Scherliess, Empirical models of storm time equatorial zonal electric fields, *J. Geophys. Res.*, *102*, 24,047, 1997.

Fejer, B. G., L. Scherliess, and E. R. de Paula, Effects of the vertical plasma drift velocity on the generation and evolution of equatorial spread F, *J. Geophys. Res.*, *104*, 19,859-19,869, 1999.

Fesen, C. G., G. Crowley, R. G. Roble, A. D. Richmond, and B. G. Fejer, Simulation of the pre-reversal enhancement in the low latitude vertical ion drifts, *Geophys. Res. Lett.*, *27*, 1851, 2000.

Groves et al., Equatorial scintillation and systems support, *Radio Sci.*, *32*, 2047, 1997.

Haerendel, G., and J. V. Eccles, The role of the equatorial electrojet in the evening ionosphere, *J. Geophys. Res.*, *97*, 1181, 1992.

Hanson, W. B., W. R. Coley, R. A. Heelis, and A. L. Urquhart, Fast equatorial bubbles, *J. Geophys. Res.*, 102, 2039, 1997.

Holzworth, R. H., R. M. Winglee, and M. C. Kelley, Whistler waves in the high-latitude magnetosphere*, J. Geophys. Res., 104,* 17369, 1999.

Huang, C. Y., W. J. Burke, J. S. Machuzak, L. C. Gentile, and P. J. Sultan, DMSP observations of equatorial plasma bubbles in the topside ionosphere near solar maximum, *J. Geophys. Res.*, *106*, 8131, 2001.

Huang, C. Y., W. J. Burke, J. S. Machuzak, L. C. Gentile, and P. J. Sultan, Equatorial plasma bubbles observed by DMSP satellites during a full solar cycle: Toward a global climatology, *J. Geophys. Res.,* 107, A12, 10.1029/2002JA009398, 2002.

Huba, J. and G. Joyce, SAMI3: A 3-D Model of the low and mid latitude ionosphere, IES Symposium 2002.

Hysell, D. L., M. C. Kelley, W. E. Swartz, and D. T. Farley, VHF radar and rocket observations of equatorial spread *F* on Kwajalein, *J. Geophys. Res.*, *99*, 15,065, 1994.

Kelley, M. C., The Earth's Ionosphere, Academic Press, Inc., 1989.

Kelley, M. C., In situ ionospheric observations of severe weather-related gravity waves and associated small-scale plasma structure*, J. Geophys. Res., 102,* 329, 1997.

Kelley, M. C., M. F. Larsen, C. LaHoz, and J. P. McClure, Gravity wave initiation of equatorial spread *F*: A case study, *J. Geophys. Res.*, *86*, 9087, 1981.

Kelley, M. C., et al., Electrical measurements in the atmosphere and ionosphere over an active thunderstorm, 1. Campaign overview and initial ionospheric results, *J. Geophys. Res., 90,* 9815, 1985.

Kelley, M. C., T. L. Franz, and G. Prasad, On the turbulent spectrum of equatorial spread F: A comparison between laboratory and space results, *J. Geophys. Res.,* 107, 1432, doi: 10.1029/2002JA009398, 2002.

Kil, H. and R. A. Heelis, Global distribution of density irregularities in the equatorial ionosphere, *J. Geophys. Res*., 103, 407, 1998.

Li, Y., Electrical and optical phenomenon over thunderstorms, Ph.D. thesis, University of Washington, 1993.

Maruyama, T., and N. Matuura, Longitudinal variability of annual changes in activity of equatorial spread *F* and plasma bubbles, *J. Geophys. Res.*, *89*, 10,903, 1984.

McClure, J. P., S. Singh, D. K. Bamgboye, F. S. Johnson, and H. Kil, Occurrence of equatorial *F* region irregularities: Evidence for tropospheric seeding, *J. Geophys. Res.*, *103*, 29,119, 1998.

Nishida, A., Geomagnetic Dp 2 fluctuations and associated magnetospheric phenomena, *J. Geophys. Res.*, *73*, 1795, 1968.

Nopper, R. W., and R. L. Carovillano, Polar-equatorial coupling during magnetically active periods, *Geophys. Res. Lett*., 5, 699, 1978.

Ott, E., Theory of Rayleigh-Taylor bubbles in the equatorial ionosphere, *J. Geophys. Res.*, 83, 2,066, 1978.

Prakash, S., Production of electric field perturbations by gravity wave winds in the E region suitable for initiating equatorial spread *F*, *J. Geophys. Res.*, *104*, 10,051, 1999.

Retterer, J. M., Theoretical model for fast equatorial bubbles, Proceedings of the 1999 Ionospheric Effects Symposium, J. Goodman, editor, 1999.

Retterer, J. M., D. T. Decker, W. S. Borer, R. E. Daniell, and B. G. Fejer, Assimilative Modeling of the Equatorial Ionosphere for Scintillation Forecasting: Modeling with Vertical Drifts, *J. Geophys. Res*., submitted, 2002.

Rino, C. L., A power law phase screen model for ionospheric scintillation, *Radio Sci.*, *14*, 1135, 1979.

Rottger, J., Equatorial spread-F by electric fields and atmospheric gravity waves generated by thunderstorms*, J. Atmos. Terr. Phys., 43,* 453, 1981.

Secan, J. A., R. M. Bussey, E. J. Fremouw, and Sa. Basu, An improved model of equatorial scintillation, *Radio Sci*., 30, 607, 1995

Senior, C. and M. Blanc, On the control of magnetospheric convection by the spatial distribution of magnetospheric conductivities, *J. Geophys. Res.*, *89,* 261, 1984

Singh, S., F. S. Johnson, and R. A. Power, Gravity wave seeding of equatorial plasma bubbles, *J. Geophys. Res.*, *102*, 7399, 1997.

Spiro, R. W., R. A. Wolf and B. J. Fejer, Penetration of high-latitude electric-field effects to low latitudes during SUNDIAL 1984, *Ann. Geophys.*, 6, 39,1988.

Sultan, P. J., Linear theory and modeling of the Rayleigh-Taylor instability leading to the occurrence of equatorial spread F, *J. Geophys. Res.*, *101*, 26,875, 1996.

Tsunoda, R. T., Control of the seasonal and longitudinal occurrence of equatorial scintillations by the longitudinal gradient in integrated *E* region Pedersen conductivity, *J. Geophys. Res.*, *90*, 447, 1985.

Ushio, T., S. J Heckman, D. J. Boccippio, H. J. Christian, and Z. I. Kwasaki, A survey of thunderstorm flash rates compared to cloud top height using TRMM satellite data*, J. Geophys. Res., 106*, 24089, 2001.

Valladares, C. E., W. B. Hanson, J. P. McClure, and B. L. Cragin, Bottomside sinusoidal irregularities in the equatorial *F* region, *J. Geophys. Res.*, *88*, 8025, 1983.

Vasyliunas, V. M., Mathematical models of magnetospheric convection and its coupling to the ionosphere, in *Particles and Fields in the Magnetosphere*, ed. by B. M. McCormac, Reidel Co. Dordrecht, Holland, 60, 1970.

Wilson, G. R., W. J. Burke, N. C. Maynard, C. Y. Huang, and H. J. Singer, Global electrodynamics observed during the initial and main phases of the July 1991 magnetic storm, *J. Geophys. Res.*, *106*, 24,517**,** 2001.

Woodman, R. F., and C. La Hoz, Radar observations of F region equatorial irregularities, *J. Geophys. Res.*, *81*, 5441, 1976.

Woodman, R. F., and E. Kudeki, A causal relationship between lightning and explosive spread F, *Geophys. Res. Lett., 11,* 1165, 1984.

Zalesak, S. T., S. L. Ossakow, and P. K. Chaturvedi, Nonlinear equatorial spread *F* - The effect of neutral winds and background Pedersen conductivity, *J. Geophys. Res.*, *87*, 151, 1982.

3. Illustrations --- C/NOFS: A Mission to Forecast Scintillation.

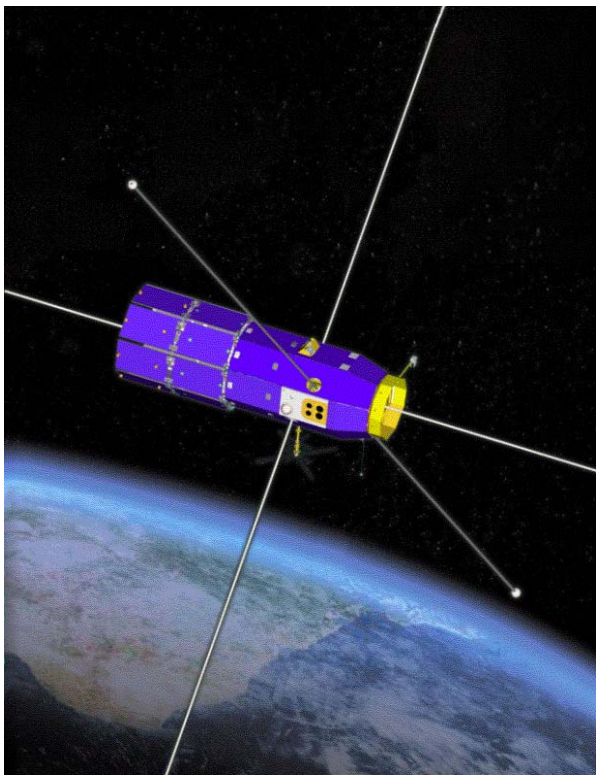

Figure 1. The C/NOFS satellite

Growth rate approximation	- Infer linear growth rate parameters along a flux tube to predict onset of R-T instability - Explain scintillation day-to day variability
Electric fields	- Separate and predict various electric field sources - Forecast strength of pre-reversal enhancement
Ambient ionosphere	- Accurately specify ambient ionosphere from C/NOFS data - Forecast several hours ahead ambient ionosphere and ascertain how prediction accuracy decreases with prediction interval
Non -linear development of plasma irregularities	- Determine irregularity strength as a function of time and space - Model and observe how equatorial plasma bubbles age, and how irregularity spectra evolve
Plasma turbulence spectrum	- Determine direction and wavelength of electrostatic plasma waves - Characterize plasma turbulence along the plasma depletions walls
Scintillation	- Determine relative influence of Bragg and Fresnel scattering - Infer phase and amplitude scintillation from in-situ density fluctuations
Scintillation climatology	- Improve scintillation climatology model, and understand physical mechanisms responsible for observed variations with space, season, activity indices, etc - Determine persistence statistics to improve long term outlook (3-day prediction)

Table 1 -- Major science topics and questions to be addressed by the C/NOFS Mission

INSTRUMENT	4. NAME	MEASURED PARAMETERS	PI & ORGANIZATION
PLP	Planar Langmuir Probe	- Electron density - Electron temperature - Power spectral densities	AFRL (D. Hunton)
IVM	Ion Velocity Meter	- Vector ion drift velocities - Ion temp - Ion composition	Univ. Texas, Dallas (R. Heelis)
NWM	Neutral Wind Meter	- Vector neutral wind velocities - Neutral composition	Univ. Texas, Dallas (G. Earle)
VEFI	Vector Electric Field Instrument	- Vector DC & AC electric fields - Magnetic fields - Relative plasma density - Optical lighting emission	NASA Goddard (R. Pfaff)
CERTO	Coherent Electromagnetic Radio Tomography	- Space-to-ground scintillations - Ne reconstruction	NRL (P. Bernhardt)
CORISS	C/NOFS Occultation Receiver for Ionospheric Sensing and Specification	- Ne profiles - Line-of-sight TEC - Space-to-space scintillation - Stratospheric refractivity	The Aerospace Corporation (P. Straus)

Table 2. List of C/NOFS instruments

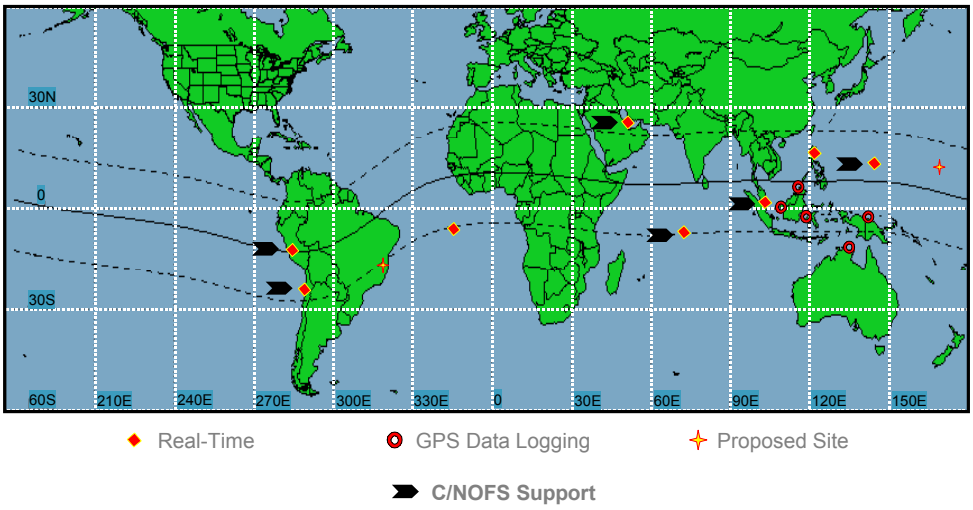

Figure 2. Existing and planned SCINDA ground stations, which are scattered around the Earth's equatorial belt. Additional stations scheduled for installation will provide critical near real-time scintillation measurements for the C/NOFS program. These measurements will enable specification of the current scintillation environment, as well as constrain and enhance the predictions of the forecast algorithms.

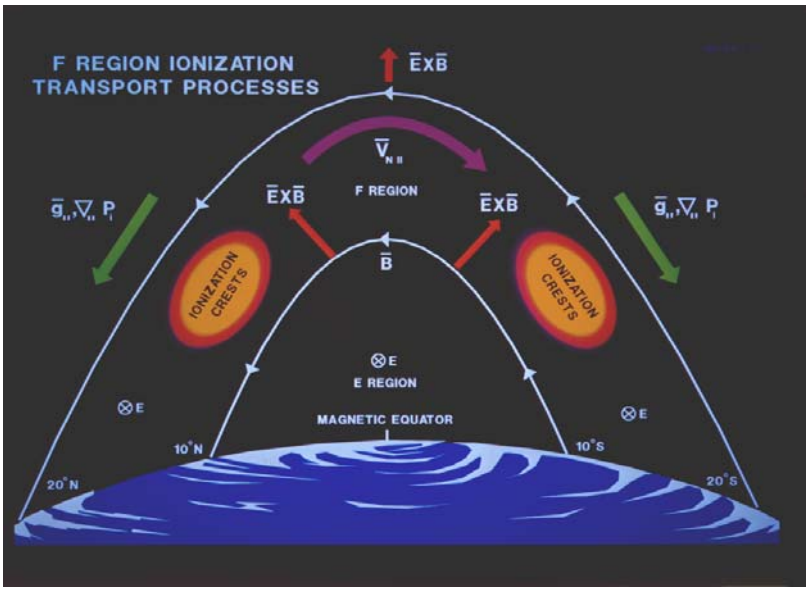

Figure 3. Schematic of the formation of the latitude variation of ionization density in the equatorial F region, known as the equatorial anomaly or the Appleton anomaly. The diagram illustrates that during daytime the eastward dynamo electric field from the E region maps along the magnetic field to F-region heights above the magnetic equator. The plasma moves upward due to **E x B** drift and then diffuses along the magnetic field to form two crests with maximum ionization density near ±15° magnetic latitude and minimum ionization at the magnetic equator.

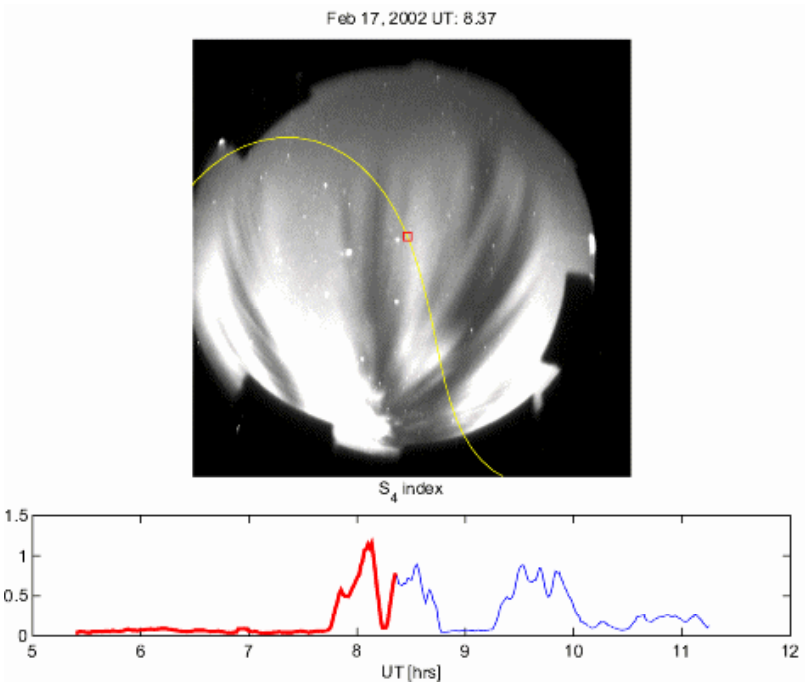

Figure 4a. Haleakala All-Sky Camera (ASC) image and GPS scintillations. Severe scintillations, as shown in the lower plot by the S_4 index from the GPS data, correlate to depleted regions of electron density (upper plot). S_4 index history shows scintillations occurred before the camera was turned on at 2020 LT. (The GPS orbit is shown on the ASC image.)

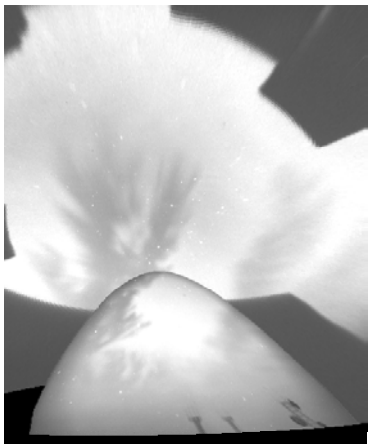

Figure 4b. Images taken by two cameras atop the Haleakala volcano in Maui, showing the equatorial ionosphere visible from this site. The lower image is from a narrow-field camera set up to look tangent to field lines at the height of the airglow layer.

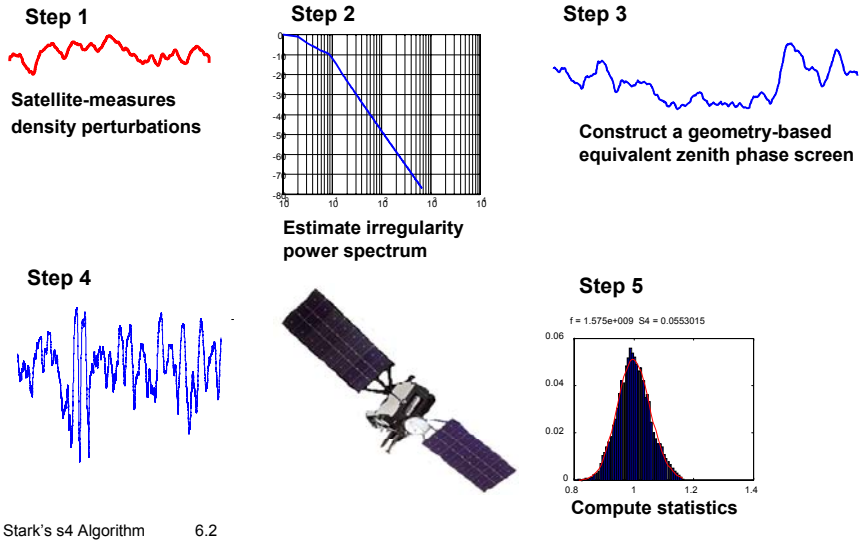

Figure 5. Algorithm for scintillation estimation. Step 1: C/NOFS satellite measures ionospheric density perturbations and returns data to the ground. Step 2: Software is used to estimate the power spectrum of the density irregularities at a given location to construct a three-dimensional irregularity model for the local ionosphere. Step 3: A thin phase screen is constructed from the irregularity model for a given transmitter-receiver link, converting the geometry to an equivalent zenith screen. Step 4: A signal is propagated through the phase screen to produce a scintillating waveform characteristic of what would be received on the ground. Step 5: Statistics are gathered to determine the estimated strength of amplitude scintillations (S_4) seen by a typical receiver.